Chapter 4

Improvement of Reactor Materials

The chapter presents a suitable amount of additives in the concrete mixture that can enhance shielding from γ-rays and neutrons. With this perception, the concrete has been prepared with different amounts of Tungsten Carbide (WC) and Boron Carbide (B_4C) additives. These samples were experimentally analyzed through γ-ray (^{60}Co) and neutron (^{252}Cf) sources at Defence Laboratory Jodhpur, Rajasthan, India. The theoretical prediction codes XCOM, MCNP, Auto-Z_{eff}, and NXcom were used to compare the present findings. In investigations shielding parameters such as; mass attenuation coefficient (μ_m), effective atomic number (Z_{eff}), effective electron density (N_{eff}), half-value layer (HVL), tenth-value layer (TVL), mean free path (MFP), and effective removal cross-section (Σ_R) were calculated. The results of this chapter show that the modified compositions are far better as compared to the pristine concrete. The results highlight that shielding parameters strongly rely on the atomic composition and density of additives of the prepared concrete.

The work from this chapter has been published in the following journal

(1) Bhargav K. Soni, Rajnikant Makwana, S. Mukherjee, Surendra Singh Barala, S. Parashari, R. Chauhan, A. S. Jodha, and K. Katovsk, Assessment of γ-ray and fast neutron shielding parameters for ordinary concrete containing different ratios of WC and B_4C, Results in Materials, 10, (2021) 100177.

4.1 Introduction

Safe working of a nuclear reactor needs sufficient and effective radiation shielding [1]. At a working stage, a reactor generates highly penetrating γ-rays and neutrons from fission and subsequent radioactive decay. Which have been absorbed and deflected using suitable shielding materials such as, concrete, lead, WC, B_4C, etc. Among the number of available shielding materials, concrete has versatile structural characteristics, inexpensive manufacturing, and high mass attenuation properties with low maintenance. It also shows adaptability with the other additive compounds of suitable densities used as supplementary cementitious materials to enhance the radiation shielding performance [2]. The type and amount of additive were primarily chosen based on the type of radiation, shape, size, a yield of the source, and the distance between a source and absorber. Apart from this, the regional availability of the additives, fabrication, durability, cost, and weight also tend to be the crucial factors [3].

Concrete is extensively used for radiation shielding purposes in nuclear power plants, particle accelerators, research reactors, nuclear waste containers, laboratory hot cells and medical facilities [4]. Water, cement, and aggregates such as gravel, sand, etc. are the basic admixture components of concrete, where elements such as H, O, Na, Mg, Al, Si, S, K, Ca, Fe, and C are the constituents [5]. Due to this, the mixture of low as well as high atomic number elements reduces the effect of both γ-rays and neutron. The elements with low-Z elements attenuate neutron due to the similarity of proton and neutron mass, whereas, heavy-Z or dense elements shows better absorption of γ-rays.

To fulfill, these well-known requirements, attention has been paid recently to the production of cost-effective, lightweight, and efficient radiation protection materials. Until now, the combination of WC and B_4C additives in concrete samples have not been investigated so far by analyzing the shielding parameters. However, B_4C based on concrete studies have been reported previously by DiJulio [6] in which they have prepared concrete by adding polyethylene beads and B_4C to the material mixture and their analysis revealed that the new concrete yields around 40% fewer neutrons, compared to standard concrete. Whereas, the studies have been performed by Ariffin [7] based on the compression strength of concrete cube with an increase in weight percent of B_4C powder additives up to 20% of the total weight of cement. They had investigated in their work that the addition of B_4C (20%) improved the mechanical and physical properties of concrete. Osman [8] has concluded from his studies that concrete containing both sepiolite and B_4C consistently showed higher radiation shielding properties than the other concretes. Castley et al., [9] have shown that B_4C can reduce secondary γ-rays in samples containing Gd_2O_3 to levels below those in borated polyethylene. Abdullah et al., [10] measured that the addition of B_4C powder to concrete has increased the ability of concrete shielding neutrons. Furthermore, the addition of 20% by wt. of B_4C significantly enhanced the neutron shielding

compared to 5% by wt. of B_4C concrete. They have also concluded from their study that, for neutron shielding application, the composition of 20% by wt. B_4C in concrete is the optimum content.

Among the available tungsten compositions, WC is of particular interest, because carbon has been used in slowing down the neutrons, reducing the final contribution in radiation [11]. Whereas, B_4C is a ceramic material commonly used to absorb the neutron. Also, a high neutron capture cross-section (3837 barns) makes boron an attractive candidate in the formulation of concrete composites [12].

In the past, work has been done to investigate the properties and parameters for the improvement in concrete composition as a radiation shielding material. Most of them have suggested different additives doping in concrete for better shielding effectiveness [13–21]. The μ_m was reported, theoretically and experimentally, for concrete containing, barite [14], different hematite-serpentine and Ilmenite-limonite [15], sepiolite minerals [13, 16], rock and concrete [17] zeolite, blast furnace slag, silica fume [18], different lime/silica ratio [19] and for seven types of concretes made to investigate for reactor technology [5]. Kharita [20] has also done a review on an admixture of the boron compounds to radiation shielding concrete. Among these, very few authors [15, 17, 19, 20] have performed to investigate for both, the γ-rays and neutron shielding for concrete compositions. Apart from this, the partial density method is used in the investigation of Σ_R for shielding materials. Dong [21] and Sayyed [13] have used the partial density method for calculating Σ_R for boron-containing resources and concrete types containing sepiolite minerals. Therefore, knowledge of the γ-rays and neutron absorption properties of concrete has become crucial for many shielding applications. In all of these findings, they have commonly used the XCOM program for the μ_m calculations. Whereas, very few authors have compared their results with simulation studies. Besides, the other shielding parameters (Z_{eff} and N_{eff}), Auto-Zeff software, and direct method have rarely been studied for concrete. By considering this, we have investigated the shielding properties of the prepared concrete samples with additives of WC and B_4C.

In view of the above, twenty-one concrete samples were prepared to examine the shielding parameters of γ-rays and neutron. The samples were prepared in a set of 1 cm, 2 cm and 3 cm average thickness, each set containing seven distinct WC and B_4C ratios in the concrete mixture, along with ordinary concrete (OC). The work has been separated into two parts considering γ-rays and neutron as separate scenarios. The interaction parameters such as; μ_m, Z_{eff}, N_{eff}, HVL, TVL, and MFP were investigated for γ-rays. This helps in examining prepared samples feasibility for γ-ray shielding. Among all, μ_m is considered as a key parameter that characterizes the dissemination and attenuation of γ-rays in the samples. Not only that, it is further used in finding other γ-ray parameters for shielding. Theoretically, μ_m were retrieved for all the samples from the XCOM program and

were simulated using the MCNP code. While the popular transmission geometry has been employed for the experimental measurements. The retrieved data from the simulation were compared with experimental measurements for the ^{60}Co γ-ray source at energies of 1.173 MeV and 1.332 MeV. Further, by considering XCOM values (μ_m), the other parameters were calculated. Moreover, the calculation of Z_{eff} of the prepared samples was performed by using the Auto-Z_{eff} software and from atomic and electronic cross-section (σ_a and σ_e) using a direct method. Recently developed computer program NXcom and MCNP simulation code were used to verify experimental measurement of Σ_R for these aforementioned samples using ^{252}Cf neutron source. The present investigation of two different additives would be very useful for improving the concrete composition to enhance the shielding properties of concrete.

4.1.1 Interaction of Radiation with Matter

According to penetration power, ionizing radiation can be categorized into two types. Which the first one comprises all charged particles like heavy ions, electrons, protons, and α particles, which interact with matter mainly via Coulombic forces [22]. This type of radiation is known as directly ionizing radiation and due to its low penetration power, it is easy to shield this radiation compared to others. The second type of ionizing radiation has high energy γ-rays and neutrons which are electrically neutral. Hence this kind of interaction with the matter by various electromagnetic mechanisms creates indirect ionization of atoms [22]. Due to its high penetration power, it passes easily through most materials and hence their shielding is relatively arduous compare to charged particles. The present work focused on the γ-ray and neutron interaction with the matter. Dominant processes leading to energy transfer in the case of γ-rays are photoelectric effect, Compton scattering, and pair production. Whereas elastic and Inelastic scattering in the case of neutrons. A brief account of these processes is given in the upcoming sections.

4.2 γ-ray Interaction with Matter

Theoretically, there are several interaction processes by which the γ-ray may interact with matter [23]. Among these only three mechanisms play a crucial role at relatively low energies (<20 MeV) that commonly come across in nuclear shielding applications, and these are

4.2.1 Photoelectric Effect

In Photo-electric effect a γ-ray may interact with an atomic electron in such a manner that it loses all of its energy and is absorbed by an orbital electron (see Figure 4.1a), if the binding energy of the γ-ray is higher than the electron, the

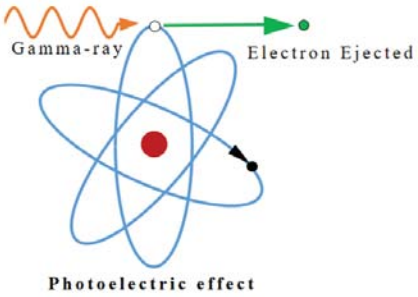

(a) A diagram illustrating the Photoelectric Effect.

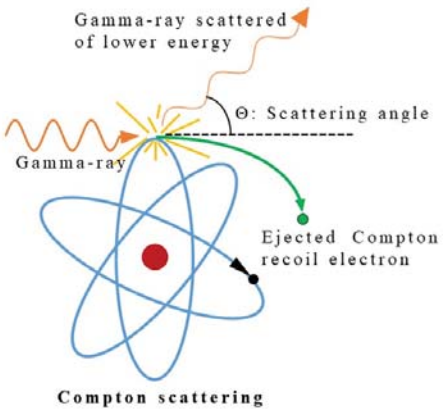

(b) A diagram illustrating the Compton Scattering.

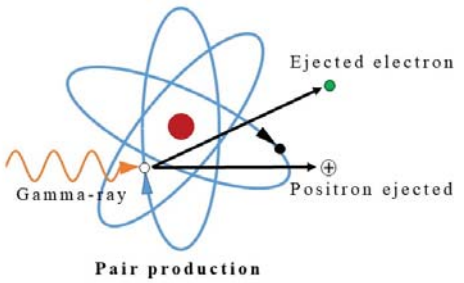

(c) A diagram illustrating the Pair Production.

Figure 4.1: γ-ray interaction with atoms.

electron will be ejected from the atom. The photoelectric effect is the primary attenuation mechanism for γ-ray below 0.1 MeV. The probability of photoelectric effect depends on γ-ray energy **E** and atomic number **Z**. The relation between cross-section with γ-ray energy and atomic number is given by;

$$\sigma \propto \frac{Z^5}{E^3}$$

4.2.2 Compton Scattering

During the interaction of γ-ray with an atomic electron of matter, the γ-ray loses only part of its energy in one interaction, resulting in a less energetic γ and a scattered electron (see Figure 4.1b). This is known as the Compton scattering process. Compton scattering is the dominant process when γ-ray energy is in the range 0.1-6 MeV [24]. The probability for this process is weakly dependent on **E** and **Z**. The relation between cross-section with atomic number is given by;

$$\sigma \propto Z$$

4.2.3 Pair Production

In the pair production, γ-ray may spontaniously create an electron-anti-electron pair, when a γ-ray has energy greater than 1.022 MeV. Mainly this interaction occurs near the nucleus. The created pair of electron and positron have equal kinetic energy but different momenta. The positron further annihilates with an orbital electron in an atom, this interaction will create two photons of 511 keV, which will travel almost directly away from one another (see Figure 4.1c). Pair production becomes dominant when the γ-ray energy is greater than ≈6 MeV. The relation between cross-section with atomic number is given by;

$$\sigma \propto Z^2$$

4.3 Neutrons Interaction with Matter

The electric field of the atoms can not affect the neutrons, because it does not have an electric charge. But the neutrons feel the strong nuclear force of the nuclei and they can interact with it through various mechanisms. Among all the feasible interaction processes for neutrons, only the below described are important for radiation shielding applications:

4.3.1 Elastic Scattering

Mainly the neutrons interact with the atomic nuclei through elastic scattering. In an elastic scattering interaction between a neutron and a target nucleus occurs, and due to this collision, the target nucleus gains some of the kinetic energy from

the interacted neutron and recoil by the conservation of momentum and energy laws. The neutron further goes on with lesser kinetic energy as far as another collision occurs and the process happens once more.

4.3.2 Inelastic scattering:

In inelastic scattering, some of the energy of the incident neutron is absorbed into the recoiling nucleus and the nucleus remains in an excited state [25]. The inelastic scattering occurs when the neutron has enough amount of energy, to raise the target nucleus to its first excited state. In this excitation process, the nuclide has raised some of its constituent nucleons to higher energy levels. The neutron further goes on with lesser kinetic energy and a change in direction. The nucleus gives up excitation energy with the emission of one or more γ-rays to reach its ground state.

4.3.3 Transmutation

In nuclear Transmutation, a neutron is absorbed by the nucleus by an element changes into another one. This newly formed atom can be stable or radioactive, in a radioactive state it can decay through several decay schemes like α, β, γ, Internal Transition (IT), or positron decay. A nuclide further decays by γ and IT transition, it will change the atomic number of the nuclide. This newly form atom will alter the atomic structure of the matter. If a large number of nuclides of the matter will transmute to other nuclides by the long and intense neutron irradiation. Then the material changes its physical or mechanical properties.

4.3.4 Radioactive Capture:

It is a very common type of reaction in which a neutron is taken in by the nucleus and leaves the compound nucleus in a highly excited state [26]. This compound nucleus will emit one or more γ-rays (without the transmutation) to return to regain the stable state, few of which can be quite energetic.

4.4 Materials and Experimental Methods

4.4.1 Material Composite Processing

To investigate the γ-rays and neutron shielding parameters, the samples were prepared according to the local manufacturing standards. All the samples were prepared using the same Ordinary Portland Cement (OPC), whereas the ratio of water/cement was kept constant, while B_4C and WC concentrations were varied systematically. In the mixing, the proportion of **OC** was kept at 80% while the remaining 20% was varied by appropriate ratios of B_4C and WC such as 0–20%, 4–16%, 8–12%, 12-8%, 16-4%, 20-0%, respectively [27]. The prepared samples

Table 4.1: Elemental Composition of prepared concrete samples used for simulations.

Sample code	Material composition	Elements (wt%)												
		H	O	Na	Mg	Al	Si	S	K	Ca	Fe	B	W	C	Density (g/cm3)
M1	80% OC + 20% WC	0.752	42.928	0.368	0.096	1.056	29.392	0.064	0.248	4.520	0.504	-	18.773	1.298	2.774
M2	80% OC + 16% WC + 04% B4C	0.752	42.928	0.368	0.096	1.056	29.392	0.064	0.248	4.520	0.504	3.132	15.018	1.940	2.673
M3	80% OC + 12% WC + 08% B4C	0.752	42.928	0.368	0.096	1.056	29.392	0.064	0.248	4.520	0.504	6.265	11.264	2.564	2.581
M4	80% OC + 08% WC + 12% B4C	0.752	42.928	0.368	0.096	1.056	29.392	0.064	0.248	4.520	0.504	9.398	7.509	3.189	2.501
M5	80% OC + 04% WC + 16% B4C	0.752	42.928	0.368	0.096	1.056	29.392	0.064	0.248	4.520	0.504	12.532	3.754	3.813	2.421
M6	80% OC + 20% B4C	0.752	42.928	0.368	0.096	1.056	29.392	0.064	0.248	4.520	0.504	15.664	-	4.437	2.300
M7	100% OC	0.940	53.660	0.460	0.120	1.320	36.740	0.080	0.310	5.650	0.630	-	-	0.090	2.341

Where, OC is Ordinary Concrete; WC is Tungsten Carbide; and B_4C is Boron Carbide.

were tagged with M1, M2, M3, M4, M5, and M6. The sample dimensions were chosen $10 \times 10 \times 1\ cm^3$ and $10 \times 10 \times 2\ cm^3$. The time duration of mixing was kept in such a manner that fresh concrete can be molded. In a typical mixing procedure, the materials were first measured with appropriate weight to reduce the time of mixing. In a bowl initially the OPC, aggregates (sand and stones) were dry mixed for approximately 2 min, and around 60% of water was added. Thereafter, a gentle mixing was done. After 2 min of mixing, the rest of the mixing water was added to it with continuously stirring for another 2 min. After 1 min of interlude, mixing for an additional 1 min was done. All the samples were mixed for a total time of 8 min and then casted in two layers with a dimension of $10 \times 10 \times 1$ and $10 \times 10 \times 2\ cm^3$. Wooden molds were covered with the hydrophobic material, in which each sample was consolidated by tapping gently [27]. After casting, concrete specimens were kept in the laboratory for about 24 h without disturbing the molds and at ambient temperature to avoid water evaporation. The prepared concrete specimens were drenched with water until the time of the experiment. It is highly recommended that adequate curing is very crucial to make heavyweight concrete. The same procedure was followed for two and three cm thick concrete slabs. Without adding any chemical compound, the **OC** sample is prepared and is labeled as M7 for corresponding thickness. The sample tags along with their density and chemical composition are given in Table 4.1.

4.4.2 Experimental Measurement

The experiment was performed at the Defence Laboratory Jodhpur, Rajasthan, India to investigate the γ-rays and neutron attenuation with these prepared concrete samples. The ORTECInc $3'' \times 3''$ NaI(Tl) scintillation detector coupled with MCA was used to detect the γ-rays photopeaks 1.173 and 1.332 MeV (16 Ci ^{60}Co source). Whereas, BF_3 detector with moderated polythene around 10 cm diameter was used to measure the attenuation of neutrons (0.536 mCi/μg ^{252}Cf source) [28]. Each concrete specimen was placed in between the point source and the detector. A schematic diagram of the ^{60}Co and ^{252}Cf experimental setups were given in the figures 4.2 and 4.3. This detector was connected to

a multichannel pulse height analyzer and operated by a personal computer from the operating room. The experiment was repeated with and without the sample for suitable times to achieve better accuracy. A detailed investigation of the present experimental data has been described in the following subsections. The overall error in the experimental measurements was calculated using error propagation rules. Mainly, the evaluation of peak areas, sample thickness measurement, density measurements and counting statistics are the source of errors in experiment.

4.5 Mathematical Description of the γ-ray and neutron shielding parameters

4.5.1 Linear Attenuation Coefficient

The linear attenuation coefficient describes the extent to which the intensity of the incident radiation beam is reduced as it traverse through a specific material. The μ provide information about the shielding effectiveness of a given material per unit thickness. The magnitude of μ is mainly depend on the thickness of material and its density. The (μ, cm^{-1}) were calculated using the Lambert-Beer's equation:

$$\frac{I}{I_0} = exp(-\mu x) \tag{4.1}$$

where, I_0 (particles/cm^2) and I (particles/cm^2) are the unattenuated and attenuated intensities of the parallel beam of γ-ray respectively when it reaches the collimated detector, and μ (cm^{-1}) is the linear attenuation coefficient of the medium. Transforming equation 4.1 in terms of logarithmic expressions on either side gives the fraction of the attenuated beam per unit thickness of the medium described as μ. Hence μ is given by Ref. [29];

$$\mu = \frac{1}{x} ln(\frac{I_0}{I}) \tag{4.2}$$

4.5.2 Mass Attenuation Coefficient

The ratio of linear attenuation coefficient (μ) to the density (ρ) of the material is known as the mass attenuation coefficient (μ_m) and has the dimension of area per unit mass (cm^3/gm).

Considering the density of material in equation 4.2 the μ transforms equation as [30]:

$$(\mu_m)_c = \sum_i W_i(\frac{I_0}{I})_i \tag{4.3}$$

The $(\mu_m)_c$ for any chemical compound or mixture of elements is given by the 'mixture rule' by assuming that the contribution of each element of the mixture

is additive. Which is described as [31],

$$W_i = \frac{n_i A_i}{\sum_i n_j A_j} \tag{4.4}$$

The above equation 4.4 consists of n_i which is the number of atoms of an i^{th} constituent element in the compound or mixture and A_i is the atomic weight of the i^{th} element [32].

4.5.3 Effective Atomic Number

The ratio of the atomic cross-section (σ_a) to the electronic cross-section (σ_e) is known as the effective atomic number (Z_{eff}). The Z_{eff} of the prepared samples were calculated from the Auto-Z_{eff} software and direct method. The details of the Z_{eff} measurement using the Auto-Z_{eff} software was given in the section 4.6.6.

Using the direct method, Z_{eff} can be determined from absorption parameters of a shielding material like a total σ_a and σ_a, determined using the $(\mu_m)_c$ value. The fraction of an incident γ-ray beam that is scattered by a single atom of the material defined as an average σ_a (cm^2/atoms) can be determined using the following relation [33]:

$$\sigma_a = \frac{1}{N_A} \sum f_i A_i (\frac{\mu}{\rho})_i \tag{4.5}$$

where N_A is the Avogadro's number (atoms g^{-1}), A_i, and W_i are the atomic mass and fractional weights of the i^{th} constituent elements of the material, respectively. The fraction of an incident γ-ray beam scattered by a single electron is defined as an average σ_e (cm^2/electron) and can be determined by the following relation [34].

$$\sigma_e = \frac{1}{N_A} \sum f_i \frac{A_i}{Z_i} (\frac{\mu}{\rho})_i \tag{4.6}$$

where, f_i is the fractional abundance of the i^{th} element of the elements in the mixture and Z_i, is the corresponding atomic number. Whereas the Z_{eff} (which is a dimensionless quantity) is directly proportional to σ_a and inversely proportional to σ_e. Therefore, by using equations 4.5 and 4.6 Z_{eff} can be formulated as follows [35]:

$$Z_{eff} = \frac{\sigma_a}{\sigma_e} \tag{4.7}$$

Also, the number of electrons per unit mass, defined as N_{eff} (electron/g) of the material, can be defined by using the previously calculated parameters (μ_m and σ_e) [36].

$$N_{eff} = \frac{\mu_m}{\sigma_e} \tag{4.8}$$

4.5.4 Half-Value Layer and Tenth Value Layer

The half value layer (HVL) (cm) and the tenth value layer (TVL) (cm) are the thicknesses of a homogeneous absorber that suppresses intensity to 50% and

90%, respectively. The relationship of these two parameters with the μ ($cm^{-}1$) can be written as [37]:

$$HVL = \frac{ln2}{\mu} \tag{4.9}$$

and

$$TVL = \frac{ln10}{\mu} \tag{4.10}$$

4.5.5 Mean Free Path

The average distance between two successive interactions of γ-rays known as MFP (cm) is determine using the following relation [38]:

$$MFP = \frac{1}{\mu} \tag{4.11}$$

4.5.6 Neutron Removal Cross-Section

A popular method of neutron removal cross-sections was employed in estimating shielding effectiveness for the neutrons. This method uses an empirical buildup factors and removal cross-sections for calculating the attenuation of neutrons, it is known as Σ_R ($cm^(-1)$). This will provide information regarding the possibility of a neutron reaction per unit length when it traverses through the medium. Besides, the Σ_R value is considered to be constant for the neutron energies between 2 and 12 MeV. This has been calculated by the following formulas [39, 40].

$$\frac{\Sigma_R}{\rho} = \sum_i w_i (\frac{\Sigma_R}{\rho})_i \tag{4.12}$$

and

$$\Sigma_R = \sum_i \rho_i (\frac{\Sigma_R}{\rho})_i \tag{4.13}$$

The values calculated from equations 4.12 and 4.13 usually have 10% accuracy, with those values which were determined experimentally [41].

4.6 Simulations

4.6.1 Execution of XCOM Program

A detailed discussion about this code is given in the section 2.5. The XCOM database is used in two ways, one is the text-based version outputs a basic text table of data. Whereas the other version is user-friendly which allows more options and features like uploading a file, graphing, and graphical tables. In the present work, we have retrieved data after completing two forms. In which the first form we have inserted a piece of general information such as, type of material: mixture with their fraction by weight for each elemental components

[1]. The program uses these input data to compute the fractions by weight of the individual atomic constituents, as well as the sum of these fractions. In the second form, we have inserted additional energies according to magnitude along with the standard energy grid. Here the additional energies are indicated by a different color in the output table to distinguish them from the standard grid values. Finally, in the output table, the γ-ray attenuation coefficients were given in the unit of cm^2/g. Which will be further used to compute μ_m, HVL, TVL, and MFP γ-ray parameters.

4.6.2 Execution of MCNP code

A Monte Carlo simulation was developed to estimate the (γ and neutron) attenuation parameters of the prepared concrete samples. This code is extensively used for simulating interactions of radiations with matter and transporting particles like neutron, γ, electron, and many other individuals or coupled-mode at a broad energy range [42]. In the present work, the simulations were separately performed for ^{60}Co and ^{252}Cf in γ and neutron transport mode shielding properties of concrete samples whose experimental setup is discussed in the 4.4.2. The schematic diagram of the experimental geometry simulated for μ_m (^{60}Co source) prediction is given in figure 4.2. Whereas, figure 4.3 shows a cross-sectional view of the simulation setup for ^{252}Cf measurements (converted) from the CAD-based Monte Carlo program:SuperMC [43–45]

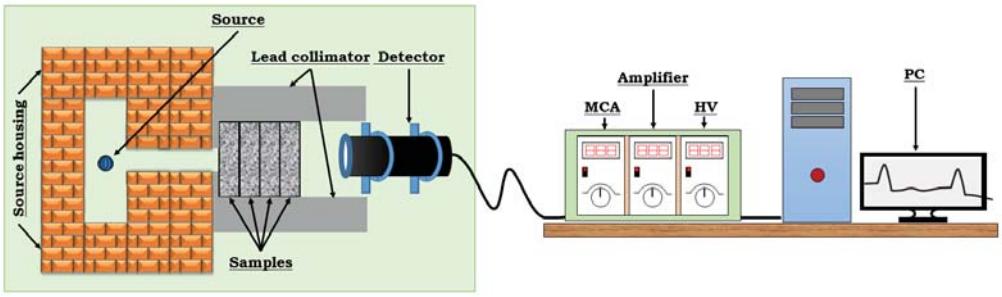

Figure 4.2: A typical arrangement of the experimental setup used for the γ-ray (^{60}Co) measurements.

The attenuation was measured by simulating all relevant physical processes and interactions before and after inserting the prepared concrete sample by considering their suitable compositions and density. The simulations assumed that the samples do not have any cracks and the composition is homogeneous throughout the volume. The F4 tally with the flux to dose conversion factor was used to obtain the particle flux and dose rates at the detector location. To reduce the runtime and statistical error, the variance reduction technique importance

[1]The materials elemental composition with their density is provided in table 4.1

biasing was used. All simulations were performed with $1e^9$ events and the tally results cleared all statistical checks and had relative errors below 1%. The specific details about the geometry, sources, and detector, and material specification are described in upcoming subsections.

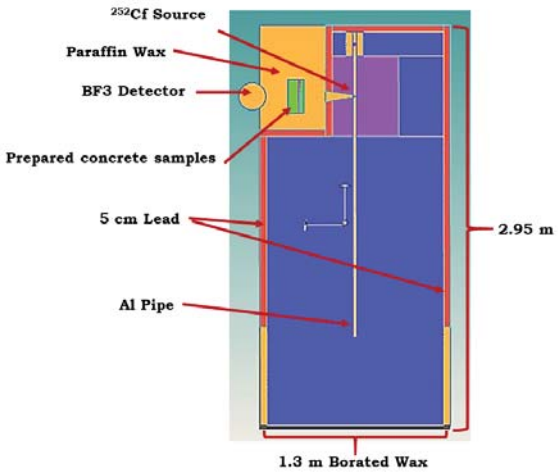

Figure 4.3: A cross-sectional view of simulation setup for neutron (^{252}Cf) measurements obtained from the CAD-based Monte Carlo program: SuperMC [43–45].

4.6.3 Geometry

For modeling purposes, the geometry of the γ and neutron experiments given in 4.4.2. A typical arrangement of the experimental setup for ^{60}CO and ^{252}Cf are illustrated in figures 4.2 and 4.3, respectively. The simulated geometry consists of two identical lead bricks with a hole in the center which is used as collimators for both the γ and neutrons. The simulated samples having a dimension of $10\times10\times1\ cm^3$ and $10\times10\times2cm^3$ with the same dimensions as the samples used for experiments. The γ and neutron weight factor is 1 in all cells (inside the defined world) and zero in the cutoff region (Outside the defined world).

4.6.4 Sources and Detector

At the center of this geometry, radioactive point source ^{60}Co and ^{252}Cf were modeled using the SDEF card. The selected γ-ray energy for ^{60}Co source are 1.173 and 1.332 MeV and the ^{252}Cf source. In both the γ and neutron simulations, the source is located at the center of the geometry. The detector (F4 tally) was located on the same axis of the source opening.

4.6.5 Material Specification

The elemental composition of the prepared samples used in simulations was determined from the mix proportions of WC and B_4C. Table 4.1 summarizes the

sample tags along with the density and chemical composition of each sample used for simulations.

4.6.6 Execution of Auto-Z_{eff} software

The functionality of the Auto-Z_{eff} software is illustrated in section 2.7.1. To calculate the effective atomic number using software first we have defined the fractional (by mass) elemental composition of concrete samples. After defining the material, energy-dependent effective atomic numbers are calculated for the material in the spectrum of energies ranging 10 keV to 1 GeV [46]. The Auto-Z_{eff} was developed for accuracy rather than calculating speed, however the computation is nonetheless brisk .

4.6.7 Execution of NXcom program

The NXcom program basically contain two database files for calculations; the first one for the fast neutrons removal coefficients and the other one for the γ-ray attenuation coefficients. Similar to XCOM and Auto-Z_{eff} program we have inserted by giving the fractions by weight of the constituents of concrete samples. After that the program calculate fast neutrons removal coefficient and listed it in output file along with the elemental composition of the inserted sample in ascending order based on the atomic numbers, as well as the weighting factors, which is, the fraction by weight of the constituents, mass removal cross-section, partial density and the macroscopic removal cross-section of the samples [47].

4.7 Results and Discussion of γ-ray and Neutron Shielding Parameters

In the present work, γ-rays and neutron shielding parameters were measured within 1-20 MeV energies. The 16 Ci ^{60}Co source was used for the γ-ray, whereas the 0.536 mCi/μg ^{252}Cf source was used for the neutron parameters measurements. The γ-ray parameters (μ, μ_m, Z_{eff}, N_{eff}, HVL, TVL and MFP) were calculated using the equations 4.1 to 4.11, while equation 4.13 was used for the neuron parameter (Σ_R). The calculated γ and neutron shielding parameters are also compared with the various simulation codes and the results of each code are presented in the upcoming sections.

4.7.1 Mass attenuation co-efficient (μ_m) of prepared concrete samples

The μ_m for incident γ-rays on concrete samples were retrieved from the XCOM program in the energy span 10^{-2} to 10^5 MeV as illustrated in figure 4.4.

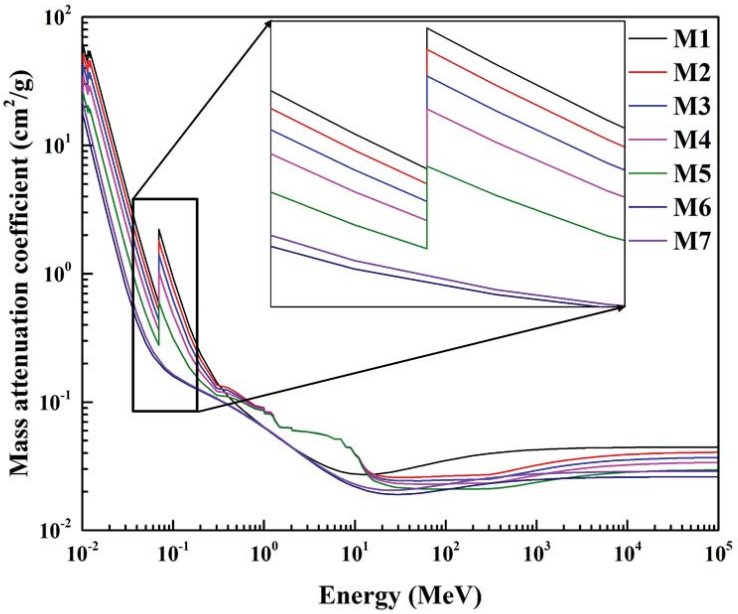

Figure 4.4: Mass attenuation coefficient of prepared concrete samples at energies 10^{-2} to 10^{5} MeV using XCOM program.

It can be delineated from figure 4.4 that the γ-ray attenuation strongly depends on the type of additive ratios (i.e. WC and B_4C). Also, it shows the functional relationship between the μ_m and γ-ray energies. For the prepared concrete samples, the values of μ_m follows the trend M6 < M7 < M5 < M4 < M3 < M2 < M1. The highest μ_m values observed for M1 among all samples, show the presence of WC additive, except in the energy range 0.3–15 MeV. However, in between this range, the presence of the B_4C additive is observed from the figure. While the μ_m value of samples M2-M5 has higher relative to the M1. But for the whole examined energy range M6 sample which has around 20% B_4C shows the lesser attenuation rest of all. These large variations occurred in the examined energy range is due to the interaction of the γ-rays with the matter, which transfers the energy to the matter near the interaction site through photoelectric absorption, Compton scattering, and pair production processes. The trend of μ_m values decreases sharply as the energy of the γ-ray reaches from 10^{-2} to 10^{-1} MeV, while energy stretches from 10^{-1}–10^{1} MeV further the value of μ_m decreases at a lower rate, after 10 MeV it slowly increases till 10^{5} MeV for the prepared concrete samples. Moreover, abrupt sharp edges appear around 10^{-1} MeV, due to the photoelectric effect near the K absorption edge of the tungsten element at 69.52 keV. It is worth mentioning that the photoelectric absorption was the dominating process at very low energy; the cross-section of this process which describes the probability of the interaction to occur varies $E^{-3.5}$ and E^{4-5}. While in the medium energies the cross-section varies with E^{-1} and Z due to the Compton scattering process. At high energy levels, the pair production cross-section is dominant and its value

varies as Z^2 [48]. For instance, the predicted values of μ_m for M1 sample at 10^{-2}, 10^{-1}, 10, and 10^5 are 35.22, 0.93, 0.06, and 0.04 cm^2/g respectively.

Further, the simulated results from XCOM and MCNP code of μ_m are graphically illustrated in figure 4.5 and tabulated in 4.2 for the better comparison.

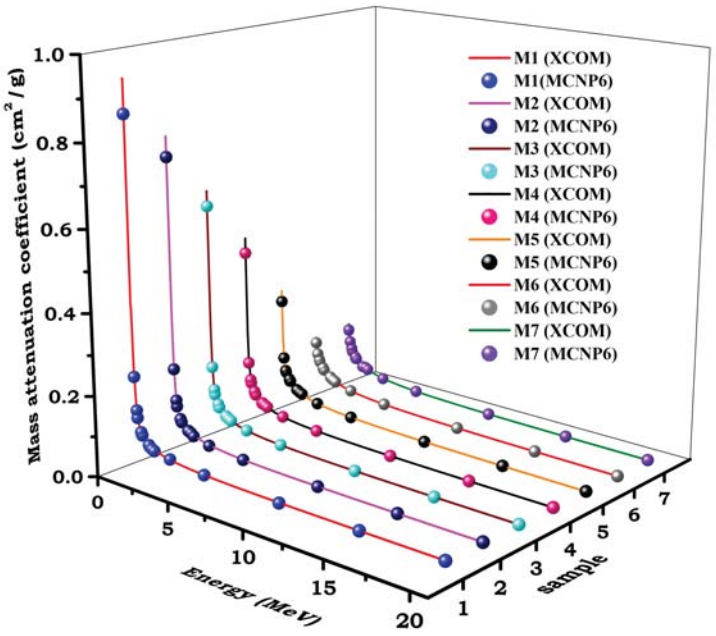

Figure 4.5: Mass attenuation coefficient of samples using MCNP code and XCOM program.

The relative deviation of the MCNP results concerning XCOM has been calculated and found below ± 9.64% for all samples.

Further, figure 4.6 show the comparisons of experimental results with MCNP and XCOM outcomes at 1.173 MeV and 1.332 MeV energies. A remarkable agreement between experimental, theoretical, and computational results was found. The maximum disagreement within all considered energies and samples was below 6.5%. This acceptable deviation can verify the accuracy of the present experiments. It may be concluded that the samples of M1-M5 show better γ-ray attenuation as compared to M6 and M7 samples. The XCOM's findings have been taken into account for further calculation of the shielding parameters.

4.7.2 Effective atomic number (Z_{eff}) and effective electron density (N_{eff}) of prepared concrete samples

The parameters Z_{eff} and N_{eff} are also played an important to understand the γ-rays attenuation properties. In the present work, Z_{eff} and N_{eff} are calculated from the direct methods (see section 4.5.3) and Auto-Z_{eff} software (see section 4.6.6). The value of the Z_{eff} and N_{eff} parameters concerning the energy as illustrated in figures 4.7 and 4.8, respectively.

Table 4.2: Comparison of mass-attenuation coefficient calculated using XCOM and MCNP program of concrete samples.

Energy (MeV)	M1		M2			M3			M4			M5			M6			M7		
	XCOM	MCNP	Diff (%)	XCOM	MCNP	Diff (%)	XCOM	MCNP	Diff (%)	XCOM	MCNP	Diff (%)	XCOM	MCNP	Diff (%)	XCOM	MCNP	Diff (%)	MCNPX	COM	Diff (%)
0.10	0.93	0.85	8.79	0.78	0.73	6.33	0.62	0.58	6.03	0.48	0.44	7.87	0.31	0.29	8.81	0.16	0.14	8.68	0.16	0.15	9.64
0.20	0.24	0.22	7.64	0.22	0.21	4.34	0.19	0.18	7.17	0.17	0.16	8.21	0.15	0.14	6.12	0.12	0.12	5.76	0.12	0.12	5.48
0.31	0.14	0.14	0.68	0.13	0.13	1.97	0.12	0.12	2.55	0.12	0.11	4.22	0.11	0.10	6.18	0.10	0.10	3.28	0.11	0.10	4.94
0.35	0.12	0.12	4.03	0.12	0.11	5.49	0.11	0.11	4.80	0.11	0.10	4.88	0.10	0.10	4.85	0.10	0.10	4.37	0.10	0.09	9.59
0.58	0.09	0.09	7.23	0.09	0.08	8.94	0.09	0.09	4.14	0.09	0.08	3.83	0.09	0.08	3.65	0.08	0.08	4.38	0.09	0.08	8.53
0.60	0.08	0.08	3.45	0.08	0.08	5.85	0.08	0.08	5.58	0.08	0.08	2.22	0.08	0.08	2.83	0.08	0.08	3.85	0.08	0.07	8.27
0.66	0.08	0.08	3.25	0.08	0.08	6.09	0.08	0.08	1.84	0.08	0.08	3.16	0.08	0.08	1.07	0.08	0.08	1.91	0.08	0.07	4.84
1.12	0.06	0.06	2.13	0.06	0.06	2.94	0.06	0.06	0.63	0.06	0.06	3.12	0.06	0.06	0.22	0.06	0.06	1.43	0.06	0.06	6.73
1.17	0.06	0.06	5.34	0.06	0.06	1.80	0.06	0.06	0.46	0.06	0.06	1.97	0.06	0.06	0.50	0.06	0.06	0.17	0.06	0.06	4.54
1.33	0.06	0.05	6.16	0.06	0.05	1.20	0.06	0.06	0.31	0.06	0.06	1.60	0.06	0.06	0.47	0.06	0.06	0.15	0.06	0.06	1.84
1.50	0.05	0.05	6.53	0.05	0.05	5.59	0.05	0.05	0.05	0.05	0.05	1.43	0.05	0.05	1.36	0.05	0.05	0.07	0.05	0.05	0.07
2.61	0.04	0.04	2.85	0.04	0.04	5.21	0.04	0.04	0.71	0.04	0.04	0.55	0.04	0.04	0.22	0.04	0.04	0.64	0.04	0.04	1.44
5.00	0.03	0.03	0.19	0.03	0.03	0.95	0.03	0.03	0.88	0.03	0.03	0.58	0.03	0.03	0.60	0.03	0.03	1.46	0.03	0.03	0.66
10.00	0.03	0.03	2.92	0.03	0.03	0.70	0.03	0.03	1.22	0.02	0.03	1.42	0.02	0.02	0.64	0.02	0.15	8.69	0.02	0.02	0.58
15.00	0.03	0.03	0.61	0.03	0.03	0.19	0.03	0.03	1.32	0.02	0.02	0.23	0.02	0.02	1.18	0.02	0.12	5.76	0.02	0.02	1.29
20.00	0.03	0.03	0.94	0.03	0.03	0.33	0.02	0.03	1.53	0.02	0.02	0.88	0.02	0.02	1.95	0.02	0.10	3.28	0.02	0.02	1.22

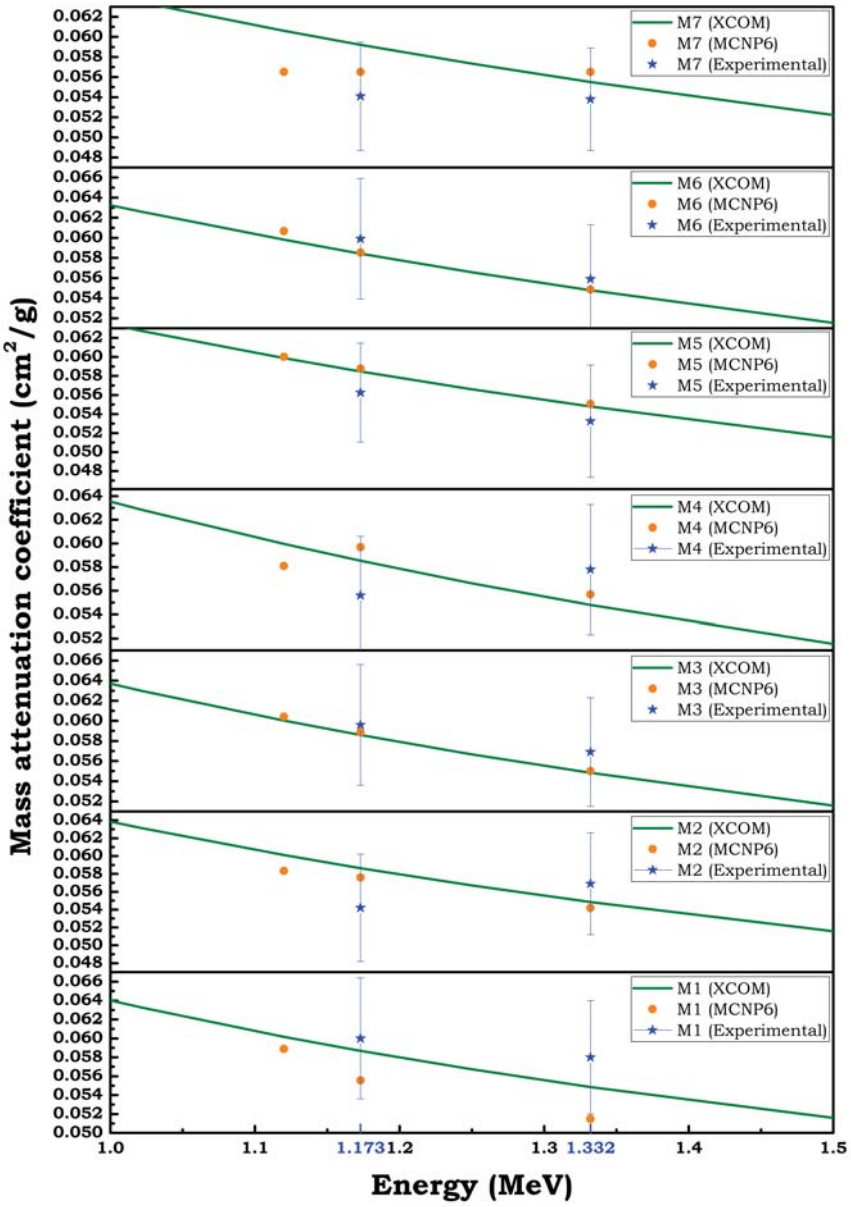

Figure 4.6: Comparisons of MCNP, XCOM, and experimental outcomes of samples using ^{60}Co source.

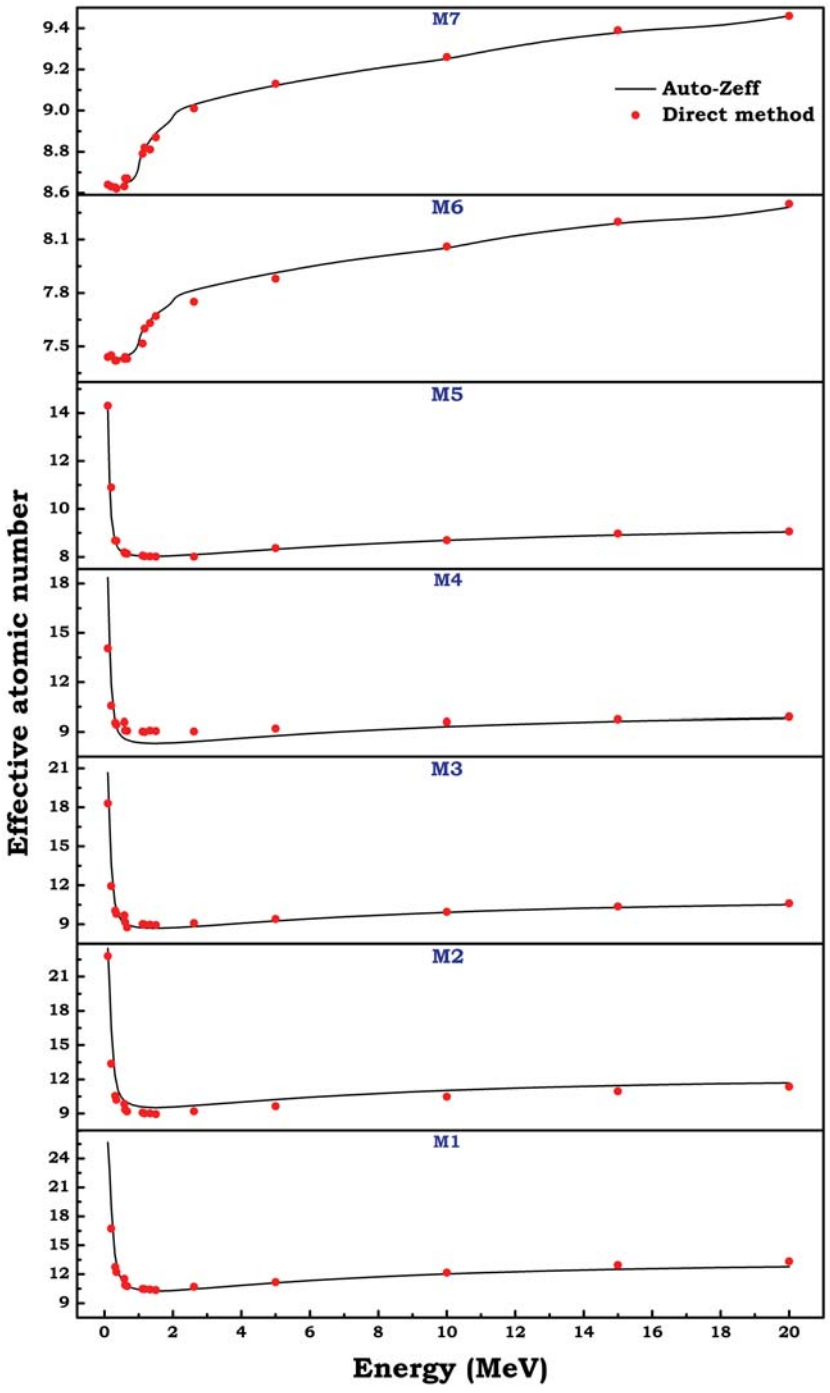

Figure 4.7: The effective atomic number of prepared concrete samples using Auto-Z_{eff} software and direct method

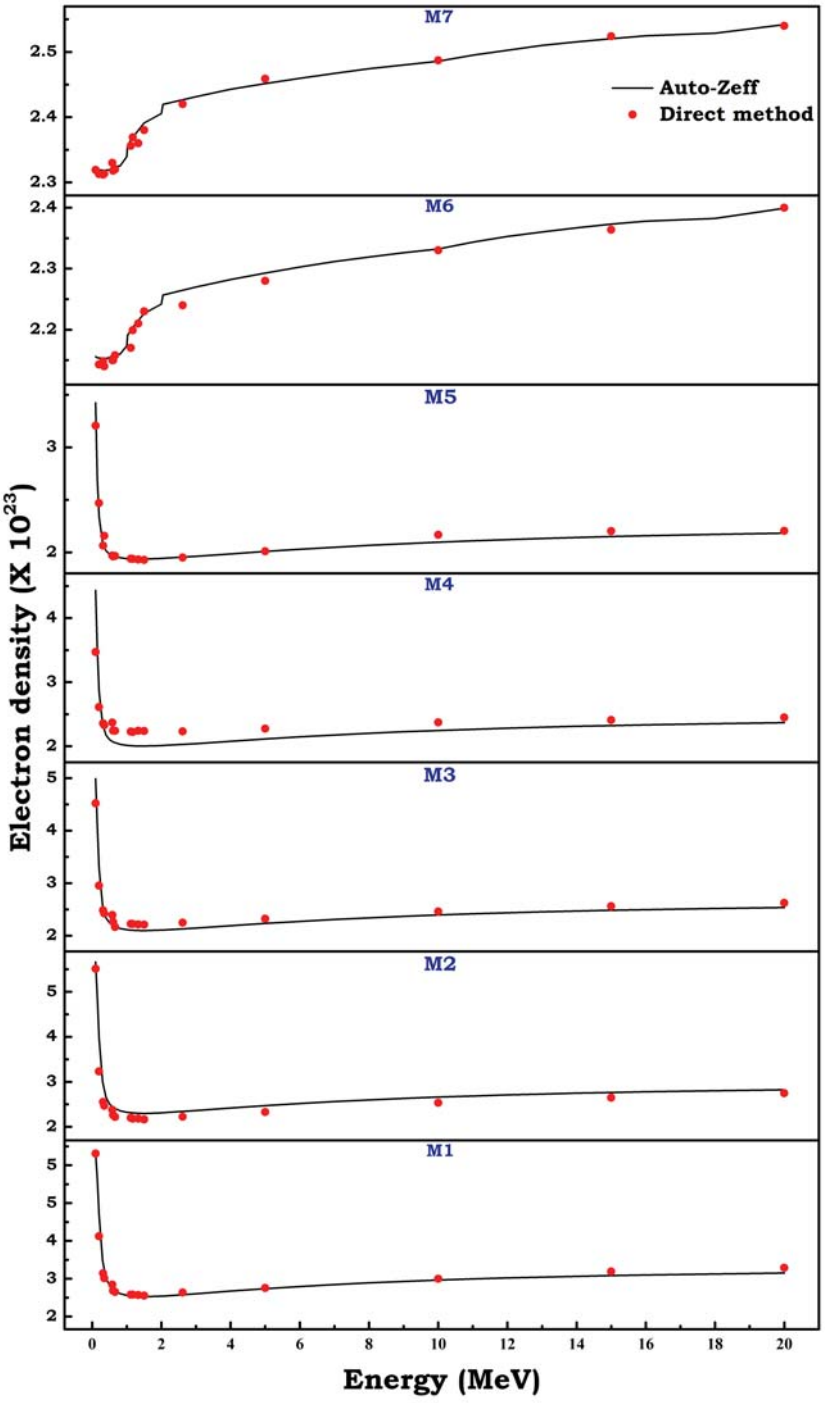

Figure 4.8: The effective electron density of prepared concrete samples using Auto-Z_{eff} software and direct method.

From figure 4.7, it is clear that the Z_{eff} computed by the direct and Auto-Z_{eff} methods are in fairly good agreement within the examined energy region. Moreover, it is also clearly evident that the trend of Z_{eff} relative to γ-rays energy is similar to the μ_m values. Therefore, this parameter was initially described in the intermediate energy region (Compton scattering dominant). There is a significant transition observed in the lower as well as in the higher energy regions (photoelectric absorption and pair-production dominant). Remarkable variations were found between the values of Z_{eff} for the samples M1 to M6, where the values were increased in the order of M6 < M7 < M5 < M4 < M3 < M2 < M1. Here, the Z_{eff} value for the M1 sample was about three and more than three times that of M6 samples. Moreover, the values of Z_{eff} for the prepared concrete samples fall in the range of 25.66–12.77, 23.46–11.66, 20.66–10.50, 18.36–9.81, 14.18–9.04, 7.44–8.28, and 8.63–9.45 for M1-M7, sequentially. As expected, from equation 4.8 parameter N_{eff} was closely related to the Z_{eff}, and their qualitative energy dependence was nearly the same for all mixtures. Here, all evaluations for Z_{eff} were considerable for the N_{eff} parameter as well. The analyzed parameters give an idea that the higher values of Z_{eff} and N_{eff} have been observed for the M1-M5 samples than that for M7 and M6, thereby showing a higher number of electrons per atom. Based on these evaluations it can be concluded that the M1-M5 samples show better γ-ray attenuating properties compared to the M6 and M7 samples.

4.7.3 Half-value layer (HVL), tenth-value layer (TVL), and mean free path (MFP) of prepared concrete samples

Sequentially in γ-ray parameter calculation, the appropriate parameters HVL and TVL were frequently used to indicate how deep a γ-ray with particular energy can penetrate any material. Hence, the calculation of these quantities have been performed with the help of equations 4.9 and 4.10 for the samples. The outcome of these parameters are shown in the figures 4.9 and 4.10.

In general, the lower the values of HVL and TVL of the material has better the shielding effectiveness [49]. Further, MFP was calculated to verify the effectiveness of the present samples as shielding material. It provides the average distance covered by the γ-rays before being interacted with the shielding material. The value of MFP was calculated from the μ by using equation 4.10.

Figure 4.11 shows the comparison of MFP for the seven prepared concrete samples. The MFP values vary with the γ-ray energy similar to that of HVL and TVL parameter values, but, based on equations 4.9 4.10 and 4.11, the HVL and TVL results are lower than MFP. In addition, the HVL, TVL and MFP values of prepared samples at different proportions were increased in the order as M6 < M7 < M5 < M4 < M3 < M2 < M1, while density of the samples were observed to be of decreasing order M1 > M2 > M3 > M4 > M5 > M7 > M6. It may be a point of greater interest as observed from figures 4.9, 4.10 and 4.11 that the

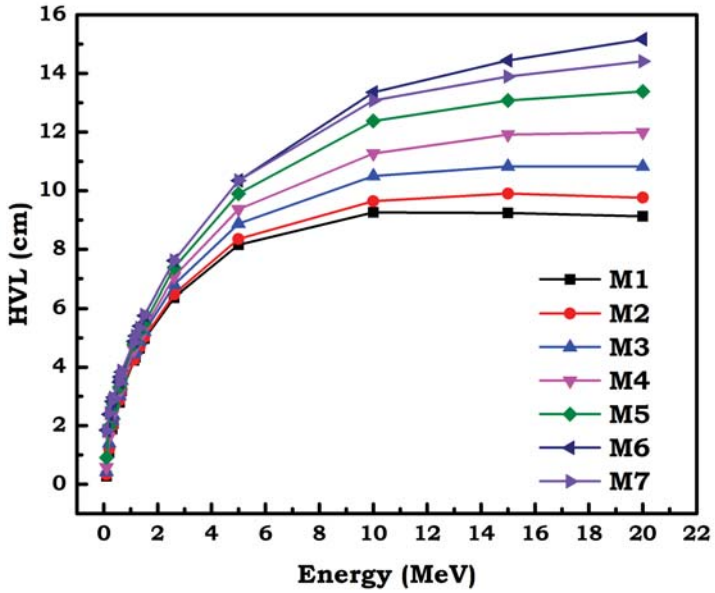

Figure 4.9: Variation in half-value layer of concrete samples using the XCOM program.

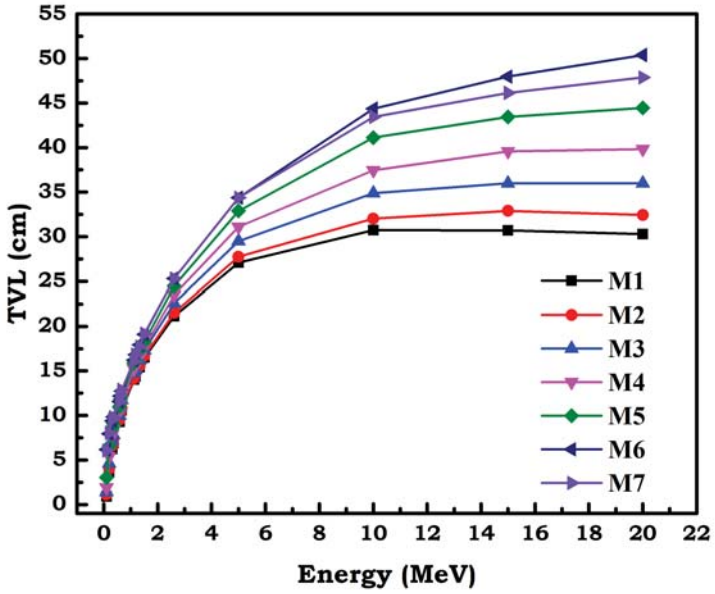

Figure 4.10: Variation in tenth value layer of concrete samples using the XCOM program.

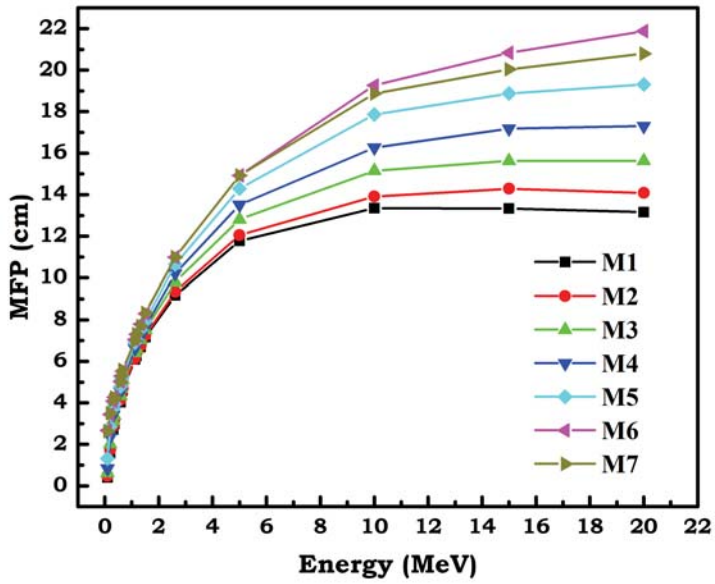

Figure 4.11: Variation in mean free path of concrete samples using the XCOM program.

trends of HVL, TVL, and MFP for the prepared samples were identical. However, their values are nearly the same at the low γ-ray energies but, increase as the energy increases for all prepared samples. While the dependence on chemical composition can be seen distinctly in the moderate and high energy regions such that, the M1 sample possesses the lowest and M6 possesses the highest values of parameters. This may be because, among the seven mixture samples, M1 (20% WC) has the best shielding properties. Also, it may be concluded that the samples M1-M5 were better shielding material than OC and M6. This shows the presence of WC and B_4C in prepared concrete samples were promising for various protection applications against γ-rays.

4.7.4 Neutron removal cross-section (Σ_R) of prepared concrete samples

Apart from γ parameters, the neutron attenuation Σ_R for the concrete samples was calculated using NXcom, MCNP code, and verified with experimental measurements. Here, the calculated values of Σ_R of concrete samples are graphically shown in figure 4.12 and listed in 4.3.

The neutron attenuation parameters Σ_R for the concrete samples was found in increased order of M7 (0.093707 cm^{-1}) < M1 (0.109742 cm^{-1}) < M2 (0.116487 cm^{-1}) < M3 (0.122549 cm^{-1}) < M4 (0.128223 cm^{-1}) < M5 (0.133496 cm^{-1}) < M6 (0.138459 cm^{-1}). The higher value of Σ_R for the M6 sample may be ascribed to possess large elemental composition of low-Z (20% B_4C); which provides a crucial

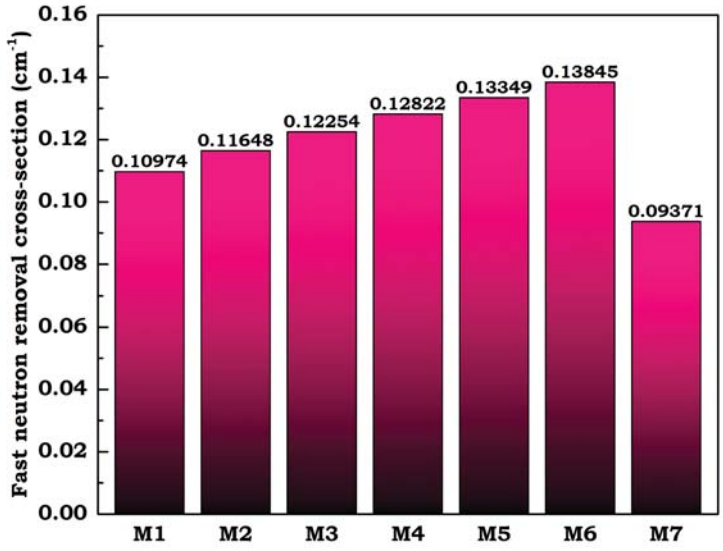

Figure 4.12: Removal cross-section of concrete samples using the NXcom program.

Table 4.3: Calculations of effective neutron removal cross-section of concrete samples.

Element	Σ_R/ρ (cm^2g^{-1})	M1 Partial density (gcm^{-3})	Σ_R/ρ (cm^{-1})	M2 Partial density (gcm^{-3})	Σ_R/ρ (cm^{-1})	M3 Partial density (gcm^{-3})	Σ_R/ρ (cm^{-1})	M4 Partial density (gcm^{-3})	Σ_R/ρ (cm^{-1})	M5 Partial density (gcm^{-3})	Σ_R/ρ (cm^{-1})	M6 Partial density (gcm^{-3})	Σ_R/ρ (cm^{-1})	M7 Partial density (gcm^{-3})	Σ_R/ρ (cm^{-1})
H	0.598	0.020845	0.012466	0.02011	0.012026	0.019419	0.011612	0.018776	0.011228	0.018169	0.010865	0.017603	0.010526	0.02162	0.012929
O	0.0405	1.189964	0.048194	1.147981	0.046493	1.10853	0.044895	1.071826	0.043409	1.037183	0.042006	1.004859	0.040697	1.23418	0.049984
Na	0.0341	0.010201	0.000348	0.009841	0.000336	0.009503	0.000324	0.009188	0.000313	0.008891	0.000303	0.008614	0.000294	0.01058	0.000361
Mg	0.0333	0.002661	0.000089	0.002567	0.000085	0.002479	0.000083	0.002397	0.00008	0.002319	0.000077	0.002247	0.000075	0.00276	0.000092
Al	0.0292	0.029272	0.000855	0.02824	0.000825	0.027269	0.000796	0.026366	0.00077	0.025514	0.000745	0.024719	0.000722	0.03036	0.000887
Si	0.0295	0.814746	0.024035	0.786001	0.023187	0.75899	0.02239	0.733859	0.021649	0.71014	0.020949	0.688008	0.020296	0.84502	0.024928
S	0.0275	0.001774	0.000049	0.001711	0.000047	0.001653	0.000045	0.001598	0.000044	0.001546	0.000043	0.001498	0.000041	0.00184	0.000051
K	0.0247	0.006875	0.00017	0.006632	0.000164	0.006404	0.000158	0.006192	0.000153	0.005992	0.000148	0.005805	0.000143	0.00713	0.000176
Ca	0.0243	0.125294	0.003045	0.120874	0.002937	0.11672	0.002836	0.112855	0.002742	0.109208	0.002654	0.105804	0.002571	0.12995	0.003158
Fe	0.0214	0.013971	0.000299	0.013478	0.000288	0.013015	0.000279	0.012584	0.000269	0.012177	0.000261	0.011798	0.000252	0.01449	0.00031
B	0.0575	0	0	0.083783	0.004818	0.161807	0.009304	0.234674	0.013494	0.302786	0.01741	0.366686	0.021084	0	0
W	0.011	0.5204	0.005724	0.401632	0.004418	0.290872	0.0032	0.187494	0.002062	0.090717	0.000998	0	0	0	0
C	0.402	0.035996	0.01447	0.051899	0.020863	0.066234	0.026626	0.079626	0.032009	0.092133	0.037037	0.103873	0.041757	0.00207	0.000832
Total			0.109742		0.116487		0.122549		0.128223		0.133496		0.138459		0.093707
Σ_R (MCNP)			0.106524		0.109995		0.115279		0.127918		0.134351		0.140138		0.092141
Σ_R (Measured)			0.108134 ± 0.005407		0.118574 ± 0.009486		0.012536 ± 0.000878		0.126325 ± 0.007581		0.132498 ± 0.005355		0.139526 ± 0.006976		0.094368 ± 0.005662

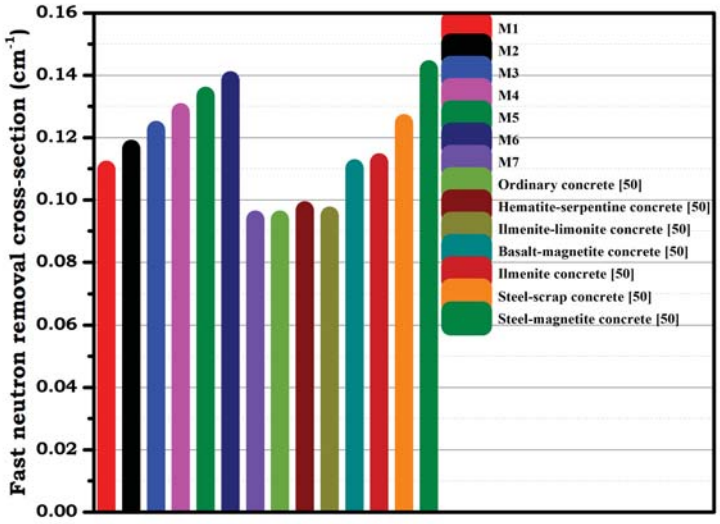

Figure 4.13: Comparison of measured removal cross-section of concrete sample with literature Bashter [50]

role in slowing down neutrons and their delayed capture. However, the difference between the Σ_R values for WC and B_4C samples (M1-M6) was relatively small. One can also see that the value is comparatively higher for OC (M7). This leads to the conclusion that the increasing percentage amount of WC and B_4C achieve better shielding properties for the neutron as shown in figure 4.12. The comparison of the fast neutron removal cross-section using different additives in concrete with literature [50] is shown in figure 4.13.

It can be observed from the comparison that M6 has slightly less neutron attenuation than steel-magnetite concrete of Bashter [50], although, it has a higher density of 5.11 (g/cm^3). While the values of Σ_R for M7 (OC) and ordinary concrete [50] predict similar results. Whereas, the prepared samples M1-M2 show better attenuation to other reported materials. Thus, the WC and B_4C can be used as an additive in the concrete.

✠ ✠ ✠ ✠

Bibliography

[1] I.I. Bashter, A.S. Makarious, et al., *Ann. Nucl. Energy*, **23**; (1) (1996) 65–71.

[2] I. I Bashter, *Ann. Nucl. Energy*, **24**; (17) (1997) 1389–1401.

[3] K. Günoglu Akkurt, A. Çalik, et al., *Bull. Mater. Sci.*, **37**; (5) (2014) 1175.

[4] A.S. Ouda, *Prog. Nucl. Energy*, **79**; (2015) 48–55.

[5] V.P. Singh, A.M. Ali, et al., *Nucl. Eng. Des.*, **265**; (2013) 1071–1077.

[6] D. D DiJulio, Cooper-Jensen, et al., *Radiat. Phys. Chem.*, **147**; (2018) 40–44.

[7] T. Ariffin, F. Nabilah, et al., *Adv. Mater. Res.*, **895**; (2014) 385–389.

[8] A. Osman, *Radiochim. Acta*, **106**; (12) (2018) 1009–1016.

[9] D. Castley, C. Goodwin, et al., *Radiat. Phys. Chem.*, **165**; (2019) 108435.

[10] Y. Abdullah, F. Ariffin, et al., *AIP Conf. Proceed.*, **1584** (1) (2014) 101–104.

[11] E.E. Hamer, A.E. McArthy, Engineering compendium on radiation shielding, in: Shielding Materials: Chapter 9.1.4 TUNGSTEN, ume II, International AtomicEnergy Agency, Berlin, Heidelberg, New York, (1970). Springer-Verlag.

[12] J.E. Martin, Physics for Radiation Protection a Handbook, second ed., Wiley VCH Verlag GmbH & Co. KGaA, Weinheim, (2006).

[13] M.I. Sayyed, H. O Tekin, et al., *Res. Phys.*, **11**; (2018) 40–45.

[14] I. Akkurt, C. Basyigit, et al., *Prog. Nucl. Energy*, **46**; (2005) 1–11.

[15] I. Bashter, A. Makarious, et al., *Ann. Nucl. Energy*, **23**; (1) (1996) 65–71.

[16] A. Osman, *Radiochim. Acta*, **106**; (12) (2018) 1009–1016.

[17] S.S. Obaid, D. K Gaikwad, et al., *Radiat. Phys. Chem.*, **144**; (2018) 356–360.

[18] I. Türkmen, Y. Ozdemir, *Ann. Nucl. Energy*, **35** ; (10) (2008) 1937–1943.

[19] A.M. El-Khayatt, *Ann. Nucl. Energy*, **37**; (3) (2010) 991–995.

[20] M.H. Kharita, S. Yousef, et al., *Prog. Nucl. Energy*, **53**; (2) (2011) 207–211.

[21] M.G. Dong, X.X. Xue, et al., *Res. Phys.*, **13**; (2019) 102129.

[22] B. Oto, N. Yildiz, et al., *Nucl. Eng. Des.*, **293**; (2015) 166–175.

[23] C. Ipbüker, H. Nulk, et al., *Nucl. Eng. Des.*, **284**; (2015) 27–37.

[24] A. Yadollahi, E. Nazemi, et al., *Prog. Nucl. Energy*, **89**; (2016) 69–77.

[25] G.F. Knoll, Radiation Detection and Measurement, (2000).

[26] T Rockwell (III), Reactor Shielding Design Manual, (1957).

[27] B. K. Soni, R Makwana, et al., *Results in Materials*, **10**; (2021) 100177.

[28] P. Narayan, L.R. Meghwal, et al., Radiological Safety Aspects in Californium-252 Source Transfer Operation, NISCAIR-CSIR, India, (2010).

[29] K. Singh, R. Kaur, et al., *Radiat. Phys. Chem.*, **47**; (4) (1996) 535–541.

[30] B. Aygün, E. S¸ akar, et al., *Res. Phys.*, **12**; (2019) 1–6.

[31] D.F. Jackson, D.J. Hawkers, *Phys. Rep.*, **70**; (1981) 169–233.

[32] J. H Hubbell, *Int. J. Appl. Radiat. Isot.*, **33**; (11) (1982) 1269–1290.

Philadelphia USA), (2003), p. 82.

[33] A. Perumallu, A. S Nageswara Rao, et al., *Can. J. Phys.*, **62**; (5) (1984) 454–459.

[34] N. Singh, K.J. Singh, *Nucl. Instrum. Methods B*, **225**; (3) (2004) 305–309.

[35] H.P. Schatzler, *Int. J. Appl. Radiat. Isot.*, **30**; (2) (1979) 115–121.

[36] F. Akman, R. Durak, *Appl. Radiat. Isot.*, **101**; (2015) 107–113.

[37] K. Günoglu, *Acta Phys Pol A*, **132**; (3) (2017) 1022–1204.

[38] M.I. Sayyed, M.Y. AlZaatreh, et al., *Res. Phys.*, **7**; (2017) 2528–2533.

[39] M.F. Kaplan, Concrete Radiation Shielding, Longman scientific and Technology, Lonman Group UK, Limited, Essex, England, (1989).

[40] A.B. Chilten, J. K Shultis, et al., *Principle of Radiation Shielding, Prentice-Hall, Englewood Cliffs, N.J.*, (1984).

[41] S. Glasstone, A. Sesonske, Nuclear Reactor Engineering, third ed., CBSPublishers & Distributors, Shahdara, Delhi, India, (1986).

[42] D.B. Pelowitz (Ed.), MCNPX Users Manual Version 2.7.0" LA-CP-11-00438, (2011).

[43] Y. Wu, FDS Team, CAD-based interface programs for fusion neutron transport simulation, *Fusion Eng. Des.*, **84** (2009) 1987–1992.

[44] W. Yican, S. Jing, et al., *Ann. Nucl.*, **82**; (2015) 161–168.

[45] R. Makwana, S. Mukherjee, et al., *Appl. Radiat. Isot.*, **127**; (2017) 150–155.

[46] M.L. Taylor, R.L. Smith, F. Dossing, R.D. Franich, Robust calculation of effective atomic numbers, *Auto-Zeff Software*, **39**; (4) (2012) 1769–1778.

[47] A.M. El-Khayatt, NXcom – A Program for Calculating Attenuation Coefficients of Fast Neutrons and Gamma-Rays, **38**; (2011), 128–132.

[48] T.T. Baris, A. Halil, et al., *Radiat. Phys. Chem.*, **153**; (2018) 89–91.

[49] G. Lakshminarayana, et al., *J. Non. Cryst. Solids*, **481**; (2018) 65–73.

[50] I.I. Bashter, *Ann. Nucl. Energy*, **24**; (17) (1997) 1389–1401.